Thin Solid Films 539 (2013) 75–80

Contents lists available at SciVerse ScienceDirect

Thin Solid Films

journal homepage: www.elsevier.com/locate/tsf

Strain enhanced ferroelectric properties of multiferroic $BiFeO_3/SrTiO_3$ superlattice structure prepared by radio frequency magnetron sputtering

Shang-Jui Chiu [a,b], Yen-Ting Liu [c], Hsin-Yi Lee [b,*], Ge-Ping Yu [a,d,**], Jia-Hong Huang [a]

[a] Department of Engineering and System Science, National Tsing Hua University, Hsinchu 30013, Taiwan, ROC
[b] National Synchrotron Radiation Research Center, 101 Hsin-Ann Road, Hsinchu Science Park, Hsinchu 30076, Taiwan, ROC
[c] Program for Science and Technology of Accelerator Light Source, National Chiao Tung University, Hsinchu 300, Taiwan, ROC
[d] Institute of Nuclear Engineering and Science, National Tsing Hua University, Hsinchu 30013, Taiwan, ROC

ARTICLE INFO

Article history:
Received 1 February 2012
Received in revised form 26 April 2013
Accepted 1 May 2013
Available online 16 May 2013

Keywords:
Superlattice structures
Interfacial strain
Radio-frequency sputtering
Bismuth ferrite

ABSTRACT

Asymmetric superlattice structures consisting of $SrTiO_3$ (STO) and multiferroic $BiFeO_3$ (BFO) sublayers were deposited on a Nb-doped STO (001) substrate with a radio frequency magnetron sputtering system. For an investigation of the effect of strain on the microstructures, ferroelectric properties and piezoelectric properties resulting from a difference of lattice parameters of the BFO sublayer, varying the thickness of the STO sublayer in a range 1–2.5 nm introduced interfacial strain into the superlattice. The epitaxial relation and strain state of films were clearly observed with a synchrotron as a source of radiation. The results of X-ray diffraction measurements clearly showed that the decrease of strain was related to the thickness of the STO substrate. A separate diffraction signal of the superlattice structure with thickness ≧1.75 nm of the STO sublayer was found, indicating a large strain relaxation in these superlattice films. The remnant polarization values P_r, piezoelectric coefficient d_{33} and leakage properties of the BFO/STO superlattice thin films that improved with increasing in-plane strain provide strong evidence of a strain-enhancement effect. The BFO/STO superlattice with a well defined crystal structure and a large strain state showed a large P_r, greater than a BFO single layer of the same thickness.

1. Introduction

Ferroelectricity and magnetism are well known to coexist for multiferroic oxide materials. They offer a prospective application in dynamic random-access memory and nonvolatile memory [1–3]. Among multiferroic oxide materials, $BiFeO_3$ (BFO) is a lead-free multiferroic material that attracts much attention because it possesses a large remnant polarization (P_r), and high Curie ($T_c = 850$ °C) and Neel ($T_N = 370$ °C) temperatures [4,5]. Wang et al. [6] showed that epitaxial BFO thin films on single-crystalline $SrTiO_3$ (STO) possess high remnant polarization (P_r, ~65 μC/cm^2) and high resistivity values (10^{10} Ω/cm).

To improve the ferroelectric properties of BFO, one approach has focused on solid solutions of BFO with other perovskite materials [7–9] or substitution of Bi and Fe elements [10–12] in BFO films. An epitaxial artificial superlattice is an efficient approach to enhance the ratio c/a, hence the ferroelectric properties of BFO films. In general, a material of perovskite type has a larger c axial lattice parameter, and deviations of cations at the octahedral interstitial sites induce favorable ferroelectric properties. A combination of material layers of perovskite type having distinct lattice parameters layer by layer epitaxially to form a multilayer would result in a mismatch between the in-plane lattice parameters, and strain from this lattice distortion becomes thereby introduced into the artificial superlattices. Kim and Nakagawara showed that a $BaTiO_3/SrTiO_3$ artificial superlattice has dielectric properties superior to those of single-layer $BaTiO_3$ and $SrTiO_3$ (STO) films [13–16]. Somenath et al. [17] prepared symmetric BFO and STO superlattices with pulsed-laser deposition to improve the ferroelectric and leakage properties of the BFO film. In this work, the relative permittivity (dielectric constant) is sensitive to the thickness of the STO sublayer. Even though the importance of the strain effect is known, the evaluation of strain in the BFO/STO superlattice structure and the alteration of the crystal structure resulting from strain are little investigated.

The ferroelectric properties of perovskite materials depend on the radii of ions in perovskite ABO_3 materials. In the tolerance factor t:

$$t = \frac{r_0 + r_A}{\sqrt{2}(r_0 + r_B)} \quad (1)$$

r_A, r_B and r_O are the radii of A, B and O atoms in perovskite ABO_3 materials. The perovskite materials with $t < 1$ which implied $r_A < r_B$ exhibit A-site driven ferroelectricity, which means that displacement of A atom in unit cell will result in "polarization" (such as $BiFeO_3$). It has shown from computational simulations that A-site driven perovskite materials are

* Corresponding author.
** Correspondence to: G.-P. Yu, Department of Engineering and System Science, National Tsing Hua University, Hsinchu 30013, Taiwan, ROC.
E-mail addresses: hylee@nsrrc.org.tw (H.-Y. Lee), gpyu@mx.nthu.edu.tw (G.-P. Yu).

0040-6090/$ – see front matter © 2013 Elsevier B.V. All rights reserved.
http://dx.doi.org/10.1016/j.tsf.2013.05.004

insensitive to epitaxial strain [18]. In our preceding work, the strain-related ferroelectric properties of a BFO superlattice structure with the A-site driven were experimentally observed [19]. Here we illustrate the effect of epitaxial strain, manipulated with the thickness of the STO sublayer, on the ferroelectric properties of BFO/STO superlattice systems.

2. Experiments

Asymmetric 10-cycle BFO/STO superlattice films were deposited on a Nb-doped STO substrate with a triple-gun radio frequency magnetron sputtering system and a computer-controlled shutter. A schematic diagram of the designed superlattice structure appears in Fig. 1. The thickness of the BFO sublayers was fixed at 6 nm; the thickness of the STO sublayer was controlled in a range from 1 to 2.5 nm to introduce a varied strain into the superlattice structure. Before deposition, the sputtering chamber was evacuated below 1.2×10^{-4} Pa to avoid contamination. Sputtering was performed at power density 1.5 W cm^{-2} for both BFO and STO with a highly purified gas (O_2 20% + Ar 80%) at a working pressure 2.05 Pa; the substrate temperature was fixed at 700 °C. With these parameters, the rates of growth of a deposited film for a BFO or STO sublayer were about 0.5 and 0.55 nm/min, respectively.

X-ray reflectivity was measured using Cu $K_{\alpha 1}$ radiation in a standard Huber two-circle X-ray diffractometer (operated at 50 kV and 200 mA). The incident light with slits in two sets yields a wave-vector resolution in the scattering plane of order 1.5×10^{-2} nm^{-1}. The principle of X-ray reflectivity is based on the recursive formalism of Parratt [20]. In this work, we fitted the reflectivity data with the Bede Mercury code [21] to determine the physical parameters of the superlattice including roughness, thickness and density. The high-resolution X-ray scattering experiments were performed at wiggler beamline BL-17B1 in the National Synchrotron Radiation Research Center (NSRRC), Hsinchu, Taiwan. Incident X-rays were focused vertically with a mirror and were made monochromatic with energy 8 keV with a Si (111) double-crystal monochromator. Using slits in two pairs between the sample and the detector, the typical scattering vector resolution in the vertical scattering plane was set to ~1×10^{-3} nm^{-1} in these experiments. For measurements of electrical properties, Pt top electrodes were sputtered onto the surface of the superlattice films at 25 °C. The ferroelectric hysteresis loop and the leakage current measurements of films were examined with a test system (TF 2000) at frequency 1 kHz and 25 °C. A commercial scanning probe micro microscope (CPII, Veeco) was used to perform measurement of piezoelectric coefficient (d_{33}).

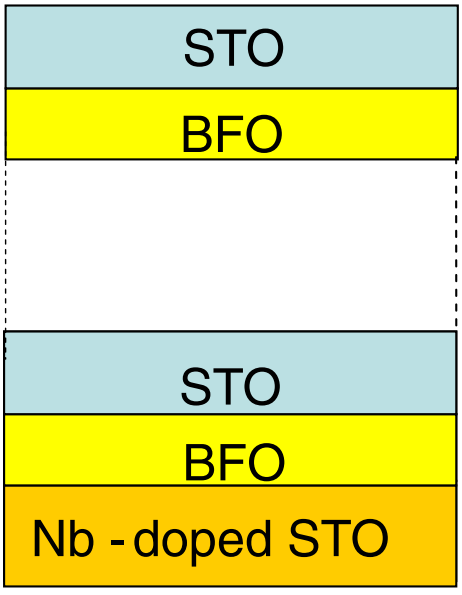

Fig. 1. Schematic diagram of the BFO/STO superlattice structure.

3. Results and discussion

Fig. 2 shows reflectivity curves (open circles) and the best-fitted results (solid lines) of BFO/STO superlattice films deposited with varied thickness of the STO sublayer. The reflectivity curves of the superlattice films with thickness less than 1.75 nm of the STO sublayer exhibit a typical shape; the presence of these clear oscillations indicates that the superlattice films have a coherent surface and interface between each sublayer and are smooth enough to produce the oscillations. The reflectivity curves present discernible superlattice peaks separated by Keissig fringes, providing evidence for a vertically periodic modulation of the composition. The best-fitted results are presented in Table 1. The fitted thickness of the sublayer in the superlattice is near the design value, which reveals that the rate of growth during deposition is stable and well controlled with the deposition system. The densities of the BFO and STO sublayers are slightly less than their bulk values, and decrease with increasing thickness of the STO sublayer. The fitted results also demonstrate that the surface and interface roughness increase with increasing thickness of the STO sublayer.

Fig. 3 presents intensity profiles of [0 0 *L*] radial scans of superlattice films with the thickness of the STO sublayer varied in a range 1–2.5 nm. The values of H, K and L in this paper are expressed in reciprocal lattice units (r. l. u.) referred to the STO lattice parameter, 0.3905 nm at 25 °C. The main line and satellite lines with accompanying clearly discernible pendellösung fringes on both sides of the main line indicate the great crystalline quality of the BFO/STO artificial superlattice structure formed on the STO substrate with RF sputtering. The superlattice films with a thickness of the STO sublayer less than 1.75 nm shows an *L*-index position increased from 1.9101 to 1.9208 with increasing thickness of the STO sublayer. This effect resulted directly from an elongation of the BFO lattice along direction [0 0 *L*] attributed to the heteroepitaxial strain.

Fig. 4 shows in-plane grazing-incidence crystal truncation-rod (CTR) spectra along direction [*H* 0 0], performed in the vicinity of the STO (200) Bragg peak of superlattice films of varied thickness of STO sublayer with high-resolution radiation from a synchrotron source, which is capable of measuring the in-plane strain of films with the grazing-incidence angle of X-rays fixed at 0.3° with respect to the sample surface. The in-plane strain state of the sample is divisible into two groups as shown in Fig. 4; the samples with STO sublayer thicknesses 1 and 1.5 nm show overlapping of the diffraction peak of the superlattice and near the STO substrate peak indicating that the BFO/STO superlattice was highly strained by the substrate. For a STO

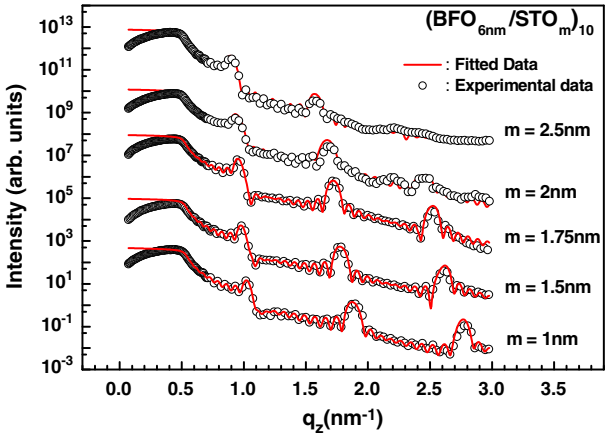

Fig. 2. Reflectivity curves (circles) of BFO/STO superlattice films deposited at varied STO sublayer thickness and their best-fitted results (solid line) as a function of momentum transfer.

Table 1
Parameters obtained from best-fitted results of reflectivity curves of BFO/STO superlattice films deposited on an Nb-doped STO substrate with varied thickness of the STO sublayer. The relative standard deviations of the fitted data are for thickness ≦2%, density ≦2% and roughness ≦6%. The thickness of the STO substrate is set as infinite; the bulk density is 5.118 g/cm^3. The bulk density of BFO is 8.354 g/cm^3 and that of STO is 5.118 g/cm^3.

STO sublayer thickness (nm)	fitted thickness (nm)		fitted density (g cm-3)		fitted roughness (nm)		
	TBF	*TSTO*	*PBFO*	*PSTO*	*σBFO/sub*	*σinterface*	*σsurface*
1	6	0.95	7.852	5.067	0.4	0.65	0.4
1.5	5.95	1.43	7.770	5.066	0. 41	0.64	0.3
1.75	5.94	1.71	7.686	4.862	4.862	0.68	0.31
2	5.89	1.97	7.602	4.709	0.42	0.8	0.58
2.5	6.01	2.41	7.519	4.657	0.41	1	0.9

sublayer thickness ≧1.75 nm, the strain in the superlattice films became much released as two diffraction lines from BFO and STO in the superlattice and also the broadening of the superlattice diffraction line are observed,

The in-plane lattice parameter of a superlattice in a cubic system is determined with this equation,

$$a = H\lambda/2\sin\theta \quad (2)$$

in which H is the Bragg location expressed in reciprocal lattice unit and θ is the measured Bragg angle. The position of the in-plane diffraction peak of the BFO sublayer in the superlattice is larger than that of bulk BFO (marked with a dashed line) in Fig. 4. The in-plane lattice parameter of superlattice films is thus smaller than the lattice parameter of bulk BFO (0.396 nm), which constitutes strong evidence for the compression of the BFO lattice by the STO substrate (and a STO sublayer). The in-plane lattice parameter of the superlattice along direction [H 0 0] and [0 K 0] that shows a similar a and b axial in-plane strain state of the superlattice films reveals that the superlattice films on the STO substrates show biaxial strain. With a thicker STO sublayer, the strain in a superlattice film is more released, and the in-plane lattice parameter increases with increasing thickness of the STO sublayer.

The in-plane strain of a superlattice film (ε_{xx}) is determined with an equation

$$\varepsilon_{xx} = (a_x - a_{x0})/a_{x0} \quad (3)$$

in which a_x is the lattice parameter of the strained layer along direction x, and a_{x0} is the average lattice parameter of bulk BFO. An in-plane lattice parameter 0.3905 nm is required for the fully strained pseudomorphic

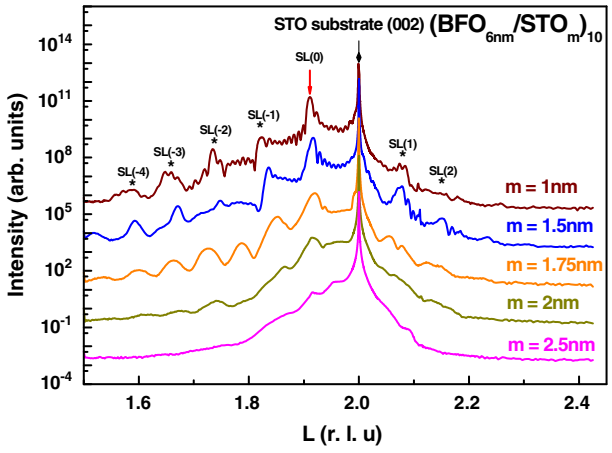

Fig. 3. Intensity distribution of a (002) radial scan of a BFO/STO superlattice film deposited with varied thickness of the STO sublayer.

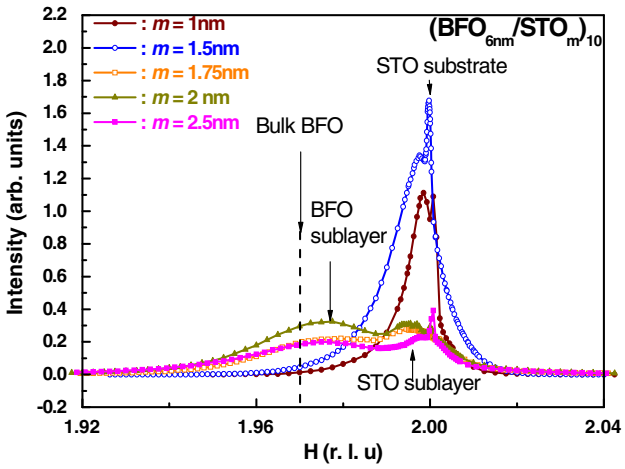

Fig. 4. Crystal truncation-rod spectrum along the (200) in-plane Bragg peak of BFO/STO superlattice films deposited with varied thickness of the STO sublayer. A dashed line marks the position of the bulk BFO diffraction peak.

growth of BFO/STO superlattices on a STO substrate. The lattice mismatch between the in-plane lattice parameter of the least strained BFO-STO bilayer, which is 0.39323 nm, and that of the STO substrate is 0.7%, which allows pseudomorphic growth for several nanometers (~30 nm) [22]. A fully strained pseudomorphic growth of each layer thus does not occur in this superlattice system during deposition, even though the thickness of individual BFO and STO layers is less than the critical thickness [23,24]. The in-plane strain of superlattice films decreases with increasing thickness of the STO sublayer as shown in Table 2. The in-plane strain diminishes rapidly in superlattice films with a STO sublayer thicker than 1.75 nm.

We performed also an in-plane azimuthal scan to investigate the epitaxial relation between the film and the substrate. An azimuthal scan of a (BFO_{6nm}/STO_{1nm}) × 10 superlattice film in the vicinity of a surface line and the substrate (200) Bragg line clearly exhibits four-fold symmetry with the same orientation as shown in Fig. 5. These results constitute firm evidence for epitaxy of the deposited layer on the substrate. No other signal was observed in the intervals between the four lines, indicating an effective alignment of a and b axes of BFO and STO unit cells along those of the STO substrate.

Fig. 6 displays the full width at half-maximum (FWHM) of the in-plane rocking curves for both BFO and STO sublayers, which increase with increasing thickness of the STO sublayer. A smaller FWHM indicates increased crystalline quality of the superlattice films. The FWHM of the film increased greatly for superlattice films with STO sublayer thicker than 1.75 nm, indicating that these films were not well aligned relative to the others.

To confirm these X-ray diffraction results, we examined the superlattice films also with a high-resolution transmission electron microscope (HRTEM). A representative HRTEM image of a (BFO_{6nm}/STO_{1nm}) × 10 superlattice structure is shown in Fig. 7. The cross-sectional TEM image on a large scale of the superlattice film clearly

Table 2
Lattice parameter, in-plane strain and ferroelectric properties of BFO_6/STO_m (nm) superlattice thin films for varied thickness of the STO sublayer.

STO sublayer thickness (nm)	L index of superlattice (r. l. u)	H index of BFO in superlattice (r. l. u)	*a*-axial lattice parameter of BFO (nm)	*εxx* (%)	2Pr (μC cm^{-2})
1	1.9101	1.9985	0.3907	−1.32	127.7
1.5	1.9173	1.9961	0.3910	−1.19	95.4
1.75	1.9208	1.9795	0.3945	−0.37	57.5
2	1.9205	1.9775	0.3949	−0.27	55.3
2.5	1.9206	1.9750	0.3952	−0.14	26.8

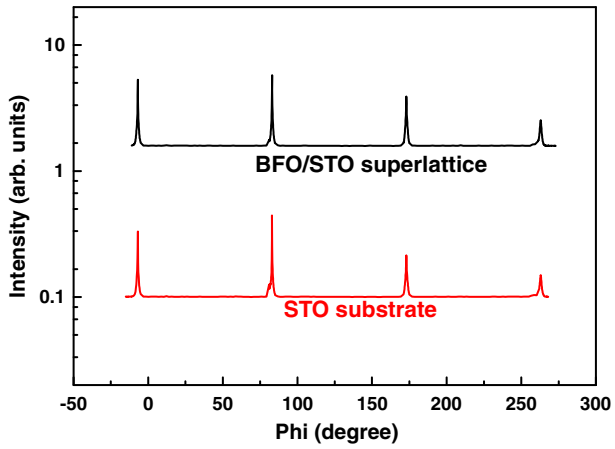

Fig. 5. Azimuthal scan (Φ scan) of the (200) Bragg line of superlattice films and the STO substrate for a BFO/STO superlattice with a STO sublayer of thickness 2 nm.

shows a well defined layer structure of BFO/STO with the STO substrate; the thickness of the sublayers agrees satisfactorily with the designed value.

Electric hysteresis loops of a BFO/STO superlattice film and a BFO single layer grown on a STO (001) substrate are given in Fig. 8 (a). The results are summarized in Table 2. The maximum attainable polarizations ($2P_r$) of BFO/STO films in a range from 127.7 to 26.83 μC cm^{-2} showed a decreasing trend with increasing thickness of the STO sublayer, but in neither case could the polarization be saturated. Fig. 8 (b) presents the relation between the in-plane strain and the polarization of superlattice

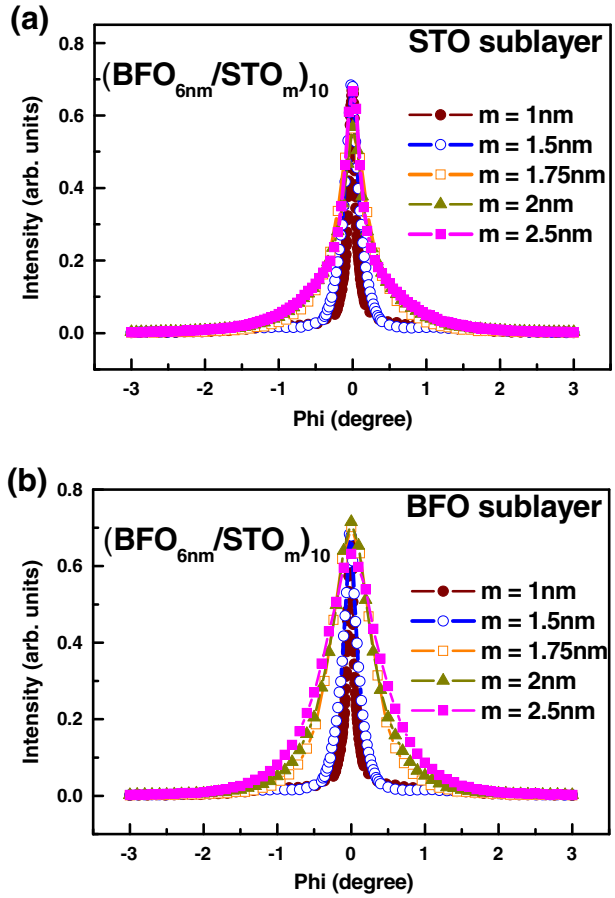

Fig. 6. Rocking curves of the in-plane (200) diffraction peak of BFO/STO superlattice films for (a) BFO and (b) STO sublayer.

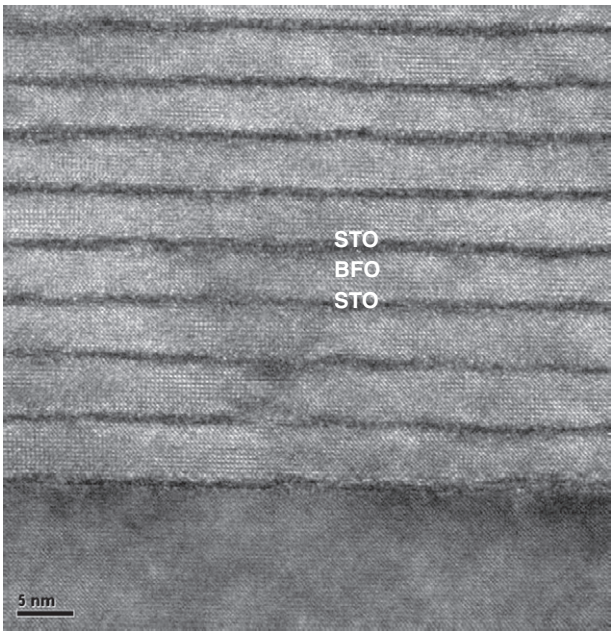

Fig. 7. HRTEM cross-sectional images showing the regular alternation of BFO and STO layers.

films. With thicknesses 1 and 1.5 nm of the STO sublayer, superlattice films show great crystalline quality with clear pendellösung fringes, and a well strained superlattice structure exhibits $2P_r$ values much larger

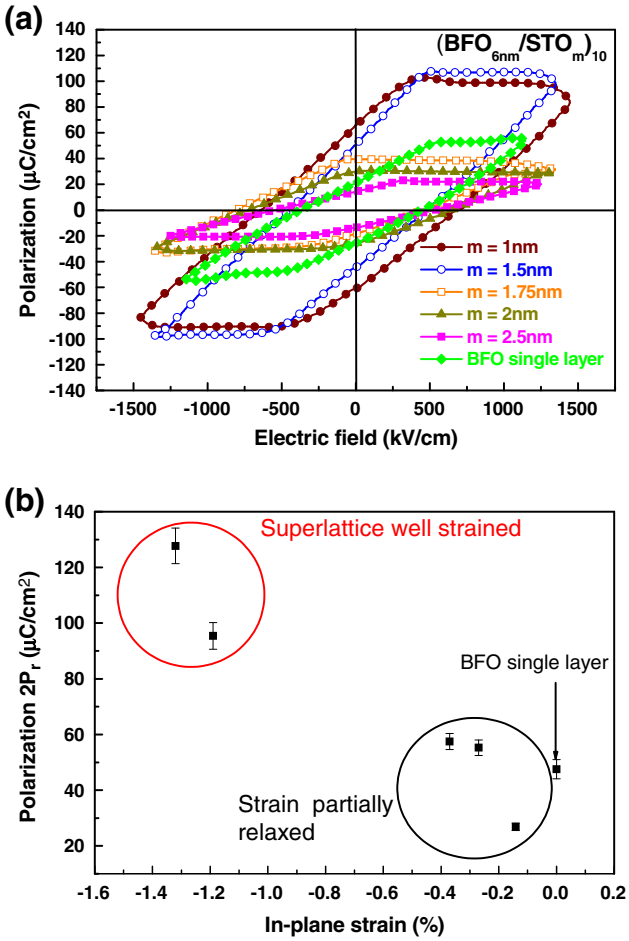

Fig. 8. (a) Electric hysteresis loops of a superlattice film and a BFO single layer (b) Variation of in-plane strain with polarization of superlattice films.

than that of a BFO single layer ~ 47.81 μC cm^{-2} for samples of the same thickness of BFO. Superlattice films of thickness ≧1.75 nm of the STO sublayer that present a poor superlattice structure with more in-plane strain relaxation in superlattice films show a rapidly decreasing value of polarization. The lowest polarization value (even lower than that of BFO single layer) of superlattice films with STO sublayer thickness 2.5 nm may be attributed to following factors: poor crystal quality, low in-plane strain, and discontinuity introduced by interface of BFO/STO sublayers of crystal structure in superlattice films. These results reveal that the ferroelectric properties of the superlattice structure are strongly affected by the in-plane strain state and the crystalline structure of these superlattice films. A crystal of high quality and with a large in-plane strain is thus essential for a superlattice film to have superior ferroelectric properties.

Fig. 9 plots the current density as a function of electric field for BFO/STO superlattice films. Superlattice films deposited at STO sublayer thicknesses 1 and 1.5 nm, which show good crystalline quality and a clear strain effect, have a small leakage density. A rapidly increasing leakage current density of the superlattice films is observed for superlattice films of thickness ≧1.75 nm of the STO sublayer.

To confirm the ferroelectric behavior of the BFO/STO superlattice films with varied thickness of the STO sublayer, we estimated also the piezoelectric properties of BFO/STO superlattice films. A ferroelectric material also has piezoelectric properties, and the piezoelectric coefficient is related to the polarization of the materials [25]. The dependence of the piezoelectric coefficient, d_{33}, and the remnant polarization on the compressive in-plane strain is shown in Fig. 10. With decreasing compressive in-plane strain in the superlattice films, the polarization and piezoelectric coefficient exhibit the same trend of a rapid decrease, especially with a thickness ≧17.5 nm of the STO sublayer of the superlattice. This result constitutes evidence that a compressive in-plane strain can enhance the polarization of BFO sublayer. The superlattice films deposited with thickness 1 nm of the STO sublayer exhibit the greatest piezoelectric coefficient (d_{33}), consistent with the results of ferroelectric properties and the effect of strain enhancement of superlattice films shown in Fig. 8(b).

Superlattice films deposited with STO sublayers of thickness 1 and 1.5 nm display a great crystalline quality, clear pendellösung fringes and a large lattice strain; these superlattice films show also excellent ferroelectric properties, piezoelectric properties and small leakage current density. For superlattice films deposited with a STO sublayer thicker than 1.75 nm, a partial relaxation of strain in the superlattice films occurs, and a large leakage current and rapid decrease of 2 P_r and d_{33} values with increasing thickness of the STO sublayer are observed. These results demonstrate that the strain state and crystalline quality

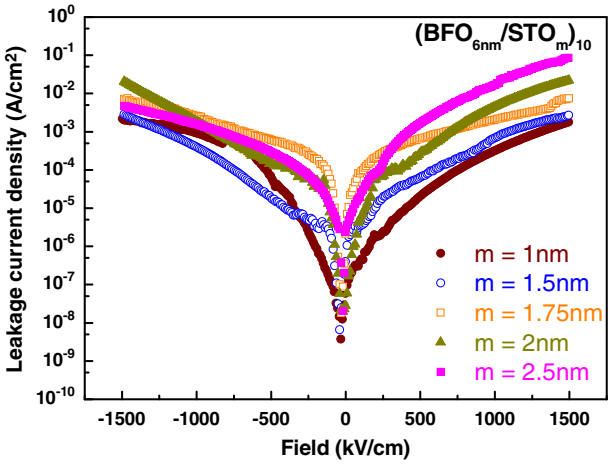

Fig. 9. Leakage current density of BFO/STO superlattice films versus electric field at varied thickness of the STO sublayer.

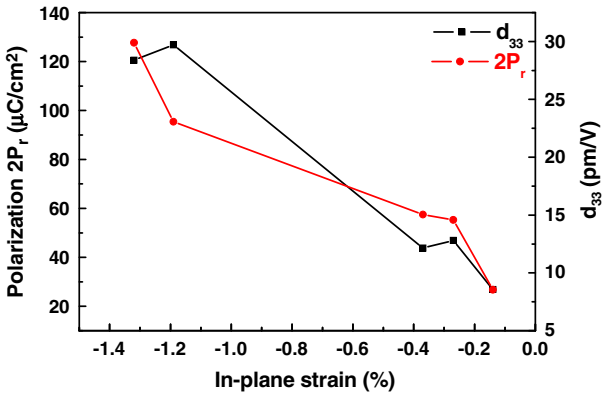

Fig. 10. Variation of d_{33} values with in-plane strain and polarization of superlattice films.

are correlated with remnant polarization and d_{33} coefficient of these films. The strain-enhanced ferroelectric properties result from the pseudo-cubic crystal structure of the BFO/STO superlattice. In calculations for the purpose of simulation [26], BFO with a rhombohedral structure shows no trend with strain, unlike BFO with a tetragonal structure. The BFO/STO superlattice well strained with STO substrates exhibits a pseudo-cubic crystal structure similar to a tetragonal structure, resulting in a clear strain effect and enhanced ferroelectric properties.

4. Conclusions

BFO/STO superlattice films with varied thickness of the STO sublayer were deposited on a (001) single-crystal STO substrate with a RF-magnetron sputtering system. With high-resolution synchrotron radiation, an azimuthal scan of a superlattice film in the vicinity of a surface peak and the substrate Bragg peak that clearly exhibit a four-fold symmetry with the same orientation provide strong evidence for an epitaxial relation between the film and the substrate. An analysis of the CTR spectra of (H 0 0) and (0 0 L) showed an increasing elongation of the BFO sublayer along [0 0 L] due to heteroepitaxial strain when the thickness of the STO sublayer was decreased. The BFO/STO superlattice with a well defined crystal structure and strain effect showed larger remnant polarization than a BFO single layer. The P_r values, piezoelectric coefficient d_{33}, and the leakage properties of the BFO/STO superlattice thin films that are enhanced with increasing in-plane strain indicate that strain can enhance both the ferroelectric and piezoelectric properties of films. A strong effect of the strain state on the ferroelectric and piezoelectric properties of a BFO/STO superlattice structure was observed in this work.

Acknowledgement

National Science Council of Republic of China supported this work under contract NSC 99-2221-E-213-002-MY2. The ferroelectric properties were measured in the Ferroelectric Laboratory, Fu Jen Catholic University.

The measurement of piezoelectric coefficient (d_{33}) is supported by Applied Nano Science Laboratory, Department of Physics, National Cheng Kung University.

References

[1] S.Y. Yang, F. Zavaliche, L. Mohaddes-Ardabili, V. Vaithyanathan, D.G. Schlom, Y.J. Lee, Y.H. Chu, M.P. Cruz, Q. Zhan, T. Zhao, R. Ramesh, Appl. Phys. Lett. 87 (2005) 102903.
[2] J. Zhang, D. Cui, H. Lu, Z. Chen, Y. Zhou, L. Li, G. Yang, S. Martin, P. Hess, Jpn. J. Appl. Phys. 76 (1997) 362.
[3] C.S. Hsi, F.Y. Hsiao, N.C. Wu, M.C. Wang, Jpn. J. Appl. Phys. 42 (2003) 544.

[4] G. Smolenskii, V. Isupov, A. Agranovskaya, N. Kranik, Sov. Phys. Solid State 2 (1961) 2651.
[5] G. Smolenskii, V. Yudin, E. Sher, Y.E. Stolypin, Sov. Phys. J. ETP 16 (1962) 622.
[6] J. Wang, J. Neaton, H. Zheng, V. Nagarajan, S. Ogale, B. Liu, D. Viehland, V. Vaithyanathan, D. Schlom, U. Waghamare, N. Spaldin, K. Rabe, M. Wuttig, R. Ramesh, Science 299 (2003) 1719.
[7] W.M. Zhu, Z.G. Ye, Appl. Phys. Lett. 89 (2006) 232904.
[8] K. Ueda, H. Tabata, T. Kawai, Appl. Phys. Lett. 75 (1999) 555.
[9] F. Huang, X. Lu, W. Lin, Xiumei Wu, Yi Kan, J. Zhu, Appl. Phys. Lett. 89 (2006) 242914.
[10] Y. Wang, Ce.W. Nan, Appl. Phys. Lett. 89 (2006) 052903.
[11] S.T. Zhang, Y. Zhang, M. Lu, C.L. Du, Y.F. Chen, Z.G. Liu, Y.Y. Zhu, N.B. Ming, X.Q. Pan, Appl. Phys. Lett. 88 (2006) 162901.
[12] J.K. Kim, S.S. Kim, W.J. Kim, A.S. Bhalla, R. Guo, Appl. Phys. Lett. 88 (2006) 132901.
[13] J. Kim, L. Kim, D. Jung, Y.S. Kim, I.W. Kim, J.H. Je, J. Lee, Jpn. J. Appl. Phys. 42 (2003) 5901.
[14] G. koebemik, W. Huessler, R. Pantoa, F. Weiss, Thin solid films 449 (2004) 80.
[15] T. Shimuta, O. Nakagawara, T. Makino, S. Arui, H. Tabata, T. Kawai, J. Appl. Phys. 91 (2002) 2290.
[16] O. Nakagawara, T. Shimuta, T. Makino, S. Arui, H. Tabata, T. Kawai, Appl. Phys. Lett. 77 (2000) 3257.
[17] B. Somenath, S.B. Krupanidhia, Appl. Phys. Lett. 90 (2007) 212902.
[18] M. Ghita, M. Fornari, Phys. Rev. B 72 (2005) 054114.
[19] S.J. Chiu, Y.T. Liu, H.Y. Lee, G.P. Yu, J.H. Huang, J. Cryst. Growth 334 (2011) 90.
[20] L.G. Parratt, Phys. Rev. 95 (1954) 359.
[21] D.K. Bowen, B.K. Tanner, Nanotechnology 4 (1993) 175.
[22] Y.C. Liang, T.B. Wu, H.Y. Lee, Y.W. Hsieh, J. Appl. Phys. 96 (2004) 584.
[23] J. Kim, Y. Kim, Y.S. Kim, J. Lee, L. Kim, D. Jung, Appl. Phys. Lett. 80 (2002) 3581.
[24] Y.C. Liang, H.Y. Lee, H.J. Liu, K.F. Wu, T.B. Wu, C.H. Lee, J. Electrochem. Soc. 152 (9) (2005) F129.
[25] A. J. Moulson and J. M. Herbert, Electroceramics Materials, Properties, Applications, John Wiley & Sons Ltd., The Atrium, Southern Gate, Chichester, West Sussex PO19 8SQ, England.
[26] C. Ederer, N.A. Spaldin, Phys. Rev. Lett. 95 (2005) 257601.